Green's functions for a layered high-contrast acoustic media

Özgür Özdemir, Hazel Yücel, Yağmur Ece Uçar, et al.

Citation: The Journal of the Acoustical Society of America **151**, 3676 (2022); doi: 10.1121/10.0011547
View online: https://doi.org/10.1121/10.0011547
View Table of Contents: https://asa.scitation.org/toc/jas/151/6
Published by the Acoustical Society of America

JASA ARTICLE

Green's functions for a layered high-contrast acoustic media

Özgür Özdemir,[1] Hazel Yücel,[2,a)] Yağmur Ece Uçar,[3] Bariş Erbaş,[3] and Nihal Ege[3]
[1]*Department of Electronics and Communication Engineering, Istanbul Technical University, Istanbul, Turkey*
[2]*Department of Computer Engineering, Başkent University, Ankara, Turkey*
[3]*Department of Mathematics, Eskişehir Technical University, Yunus Emre Campus, Eskişehir, Turkey*

ABSTRACT:
A parametric approach based on parametric analysis of the acoustical properties of a layered media is proposed to derive a reduced layered Green's function. The approach relies on the smallness of one of the problem parameters and allows a simpler form of Green's function by disregarding the smaller parametric terms. Several illustrative examples comparing the amplitudes of exact and reduced Green's function for small parameter of density ratio in various source and observation location setups are presented. It is demonstrated that the CPU times calculated at different points decrease considerably for the reduced Green's function, further justifying the presented method.
 https://doi.org/10.1121/10.0011547
(Received 28 December 2021; revised 18 April 2022; accepted 14 May 2022; published online 2 June 2022)
[Editor: James F. Lynch] Pages: 3676–3684

I. INTRODUCTION

In the photoacoustic and ultrasound imaging techniques, the measured acoustics waves are converted to image by using the physical model of wave propagation which commonly involves the Green's function. The major impact on the speed of the imaging algorithms come from the efficient calculation of Green's function. In many practical applications the region is composed of different homogeneous environments forming what is called layered media. For layered media, acoustic layered Green's functions comprising acoustic and physical parameters of layers cannot straightforwardly be expressed as analytical formulas but are expressed as Sommerfield integrals containing spectral domain Green's function. In layered media, a Sommerfield integral involves highly oscillatory and slowly attenuating integrands which makes numerical calculations difficult and requires long computation times for stable solutions.[1–4]

There are various studies in literature which focus particularly on accelerating the calculation of Green's function for electromagnetic waves in layered media such as acceleration by transformations[5] or reducing the integral representation to an analytic or semi-analytic form.[6–10] The spectral Green's function coefficients in the discrete complex image method (DCIM), developed to represent the Green's function in an analytical form, are expressed as a sum of complex exponentials and written in an analytical form using the Sommerfeld identity.[7,8,11,12] The calculation of complex exponentials, i.e., the spherical wave amplitudes, are, then, carried out through the use of Prony or GPOF (generalized pencil of function) methods.[8,13,14] Although DCIM gives favourable results in near field expressions, its rate of success decreases in far field values. To reduce the error in far field expression two or three-level DCIMs are suggested.[11] The rational function fitting method is proposed as an alternative to DCIM to accurately calculate the far field values of layered Green's function.[10,15,16] In this method, while the Green's function is expressed as the sum of the cylindrical waves, the amplitudes of the waves are calculated as the solution of an eigenvalue problem or by a vector fitting algorithm. Various other methods, including k-space models, have also been developed to tackle with the solution of Green's function for inhomogeneous and multilayered media.[1,17]

In this work, we have proposed to use of parametric investigation of acoustics layered Green's functions in high contrast environment to reduce the computation times. A parametric analysis approach relies on the introduction of small parameters inherent in the physics of the problem thereby reducing the exact formulations to the approximate ones. This enables simpler forms of the solutions which are otherwise intractable. Such an approach of parametric analysis is common, say, in dynamic elasticity in the investigation of vibration problems of multicomponent rods,[18] layered elastic structures,[19] and drilling of wells in oil industry,[20] to name but a few. To the best of our knowledge, parametric analysis has not been applied to the Green's function of layered acoustic medium. To this aim, we introduce a small parameter into the problem by taking into account the ratios of the layer densities, from which a reduced form of the Green's function may be obtained on employing the high contrast in magnitudes of the introduced parameter. Ignoring the asymptotically smaller terms in the kernels results in a simplified form of the layered Green's function which will be called as the reduced Green's function. The proposed analysis not only permits a better understanding of the underlying physics of the problem, but may also lead to faster numerical computations due to a shortened form. We should note that to perform parametric analysis for a single parameter, only the ratio of densities in the problem

[a)]Electronic mail: ahazely@baskent.edu.tr

https://doi.org/10.1121/10.0011547

is assumed to have high contrast, while the rest of the acoustic parameters are assumed to be in the same order.

This approach could be extended to more general setups including variation of wave speed, yet, the methodological approach will virtually be the same.

The rest of the paper is organized as follows: In Sec. II, the Green's function of layered acoustic media is presented and parametric analysis is explained in Sec. III. Numerical examples are presented to show the efficiency of the proposed approach.

II. GREEN'S FUNCTION FOR LAYERED ACOUSTIC MEDIA

We consider a layered acoustic medium consisting of N homogeneous layers which extend infinitely in the transverse direction, as shown in Fig. 1. Each layer is characterized with speed of sound c_m and density ρ_m. The first interface is assumed to be placed along the axis $z=0$ and the remaining interfaces are located at $z=h_m$, $m=1,2,\ldots,N-1$.

The source is assumed to be located in the first layer at $r'=(x',z')$. The Green's function of the N–layered medium can be expressed in spectral integral form as follows:

$$
\begin{aligned}
G_{11} &= \frac{1}{2\pi}\int_0^\infty \left(e^{-k_{z_1}|z-z'|} + R_N e^{-k_{z_1}|z+z'|}\right) \\
&\quad \times \frac{\cos\left(k_x|x-x'|\right)}{k_{z_1}} dk_x, \quad z \in \text{layer } 1, \\
G_{12} &= \frac{1}{2\pi}\int_0^\infty \left(C_1^{(2)}\sinh(k_{z_2}z) + C_2^{(2)}\cosh(k_{z_2}z)\right) \\
&\quad \times \frac{\cos\left(k_x|x-x'|\right)}{k_{z_1}} dk_x, \quad z \in \text{layer } 2, \\
&\vdots \\
G_{1m} &= \frac{1}{2\pi}\int_0^\infty \left(C_1^{(m)}\sinh(k_{z_m}z) + C_2^{(m)}\cosh(k_{z_m}z)\right) \\
&\quad \times \frac{\cos\left(k_x|x-x'|\right)}{k_{z_1}} dk_x, \quad z \in \text{layer } m, \\
&\vdots \\
G_{1N} &= \frac{1}{2\pi}\int_0^\infty C_2^{(N)} e^{k_{z_N}z} \frac{\cos\left(k_x|x-x'|\right)}{k_{z_1}} dk_x, \\
&\quad z \in \text{layer } N.
\end{aligned} \tag{1}
$$

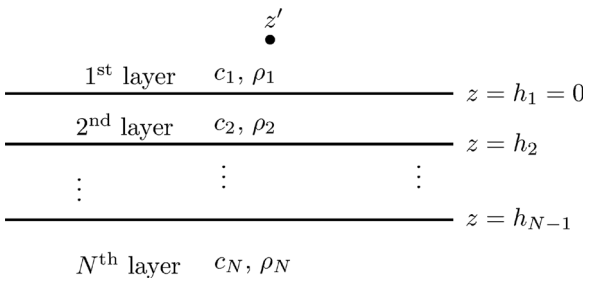

FIG. 1. Configuration of N-layered acoustic medium.

R_N, $C_1^{(m)}$, and $C_2^{(m)}$ are the unknown coefficients to be determined. Note that the sine and cosine functions are used to represent the kernel of Green's function in the intermediate layers replacing the exponential function. Finally, in the last layer, there is only one exponential term which represents outgoing waves since the radiation boundary condition only allows outgoing waves at infinity. In addition to the radiation condition, the Green's function also satisfies the following continuity conditions at each interface:

$$
\lim_{\mathbf{r}\to S^-} G(\mathbf{r}',\mathbf{r}) = \lim_{\mathbf{r}\to S^+} G(\mathbf{r}',\mathbf{r}), \tag{2}
$$

$$
\lim_{\mathbf{r}\to S^-} \frac{1}{\rho^-}\frac{\partial G(\mathbf{r}',\mathbf{r})}{\partial \mathbf{n}} = \lim_{\mathbf{r}\to S^+} \frac{1}{\rho^+}\frac{\partial G(\mathbf{r}',\mathbf{r})}{\partial \mathbf{n}}. \tag{3}
$$

Here, S is the boundary surface and ρ^- and ρ^+ are the densities for the lower and upper layers, respectively. The unknown coefficients in the kernel can be determined matching these continuity conditions at each interface. The propagation constant k_{z_m} in Eq. (1) is defined as

$$
k_{z_m} = \begin{cases} -i\sqrt{k_m^2 - k_x^2}, & |k_x| < |k_m|, \\ \sqrt{k_x^2 - k_m^2}, & |k_x| > |k_m|, \end{cases} \tag{4}
$$

where k_m is the wavenumber in the mth layer.

III. PARAMETRIC ANALYSIS

In this work, we aim to simplify the structure of the layered Green's functions and reduce the computational cost through the reduction of the number of terms in its kernel. To this end, a parametric analysis is performed to assess the influence of the layer's densities on the solution to the Green's function. In order to simplify the analysis, we introduce a non-dimensional spatial wavenumber K_x, spectral frequency Ω_m together with thickness d_m representing the distance between two consecutive layers, where h_m is the layer coordinate, as follows:

$$
\Omega_m = k_m d_m, \quad K_x = k_x d_m, \quad d_m = |h_m - h_{m-1}|. \tag{5}
$$

We should point out that when the medium is two-layered, d_m can be taken as the distance from the source to the interface. The ratios of the layers' densities as a parameter in parametric analysis and the nondimensional constant $\mathcal{H}_m$ are also defined as follows:

$$
\begin{aligned}
&\mathcal{H}_m = \frac{h_m}{d_m}, \quad \rho_{mn} = \frac{\rho_m}{\rho_n}, \quad m = 1,\ldots,N-1, \\
&n = m+1,\ldots,N.
\end{aligned} \tag{6}
$$

Using the non-dimensional quantities, Eq. (4) may be rewritten in the form

$$
K_{z_m} = \begin{cases} -i\sqrt{\Omega_m^2 - K_x^2}, & |K_x| < |\Omega_m|, \\ \sqrt{K_x^2 - \Omega_m^2}, & |K_x| > |\Omega_m|, \end{cases} \tag{7}
$$

where $K_{z_m} = k_{z_m} d_m$. On inserting the nondimensional quantities (5)–(7) in Eq. (1), the unknown coefficients, R_N, $C_1^{(m)}$, $C_2^{(m)}$, may be determined by matching the continuity conditions (2) at each of the interfaces. The resulting system of linear equations can be written as a matrix equation given by

$$\begin{bmatrix} A_{11} & A_{12} & & 0 & \\ & \ddots & \ddots & & \\ & & A_{jj} & A_{j,j+1} & \\ & 0 & & \ddots & \ddots \\ & & & A_{N-1,N-1} & A_{N-1,N} \end{bmatrix} \begin{bmatrix} R_N \\ C_1^{(2)} \\ C_2^{(2)} \\ \vdots \\ C_2^{(N)} \end{bmatrix} = \begin{bmatrix} -e^{-K_{z_1} z'} \\ -K_{z_1} e^{-K_{z_1} z'} \\ 0 \\ \vdots \\ 0 \end{bmatrix}. \tag{8}$$

Note that the matrix of coefficients on the left hand side of Eq. (8) has the structure of a banded block matrix which is a result of the continuity conditions at the interface of each layer. The entries A_{ij} in the matrix of coefficients are defined as

$$A_{11} = \begin{bmatrix} e^{-K_{z_1} z'} \\ -K_{z_1} e^{-K_{z_1} z'} \end{bmatrix}, \quad A_{12} = \begin{bmatrix} 0 & -1 \\ -\rho_{12} K_{z_2} & 0 \end{bmatrix}, \tag{9}$$

$$A_{jj} = \begin{bmatrix} \sinh(K_{z_j} \mathcal{H}_j) & \cosh(K_{z_j} \mathcal{H}_j) \\ K_{z_j} \cosh(K_{z_j} \mathcal{H}_j) & K_{z_j} \sinh(K_{z_j} \mathcal{H}_j) \end{bmatrix}, \tag{10}$$

$$A_{j,j+1} = \begin{bmatrix} -\sinh(K_{z_{j+1}} \mathcal{H}_j) & -\cosh(K_{z_{j+1}} \mathcal{H}_j) \\ -\rho_{j(j+1)} K_{z_{j+1}} \cosh(K_{z_{j+1}} \mathcal{H}_j) & -\rho_{j(j+1)} K_{z_{j+1}} \sinh(K_{z_{j+1}} \mathcal{H}_j) \end{bmatrix}, \tag{11}$$

$$A_{N-1,N} = \begin{bmatrix} -e^{K_{z_N} \mathcal{H}_{N-1}} \\ -\rho_{(N-1)N} K_{z_N} e^{K_{z_N} \mathcal{H}_{N-1}} \end{bmatrix}, \tag{12}$$

where the index j runs from 2 to $N-1$ with $N \geq 3$. The entries A_{11} and $A_{N-1,N}$ are 2×1 matrices, therefore, the size of the coefficient matrix A becomes $2N-2 \times 2N-2$. Note that for $N=2$, we take the first and last block matrices having the size of 2×1 due to radiation conditions. As it seen from Eqs. (9)–(12), the entries of the matrix of coefficients in Eq. (8) are functions of the ratios of the layer densities $\rho_{j(j+1)}$. Thus, the kernel of the Green's function depends on the ratio of the layers densities $\rho_{j(j+1)}$. Let us consider the configuration in which the densities are of increasing order of magnitudes, that is, $\rho_1 \ll \rho_2 \ll \cdots \ll \rho_N$. We should note that any configuration can be reduced to this form by rearranging the rows of Eq. (8). The magnitudes of the non-dimensional density ratios defined as $\rho_{iN} = \rho_i / \rho_N$, $i = 1, \ldots, N$, are therefore ordered as $\rho_{1N} \ll \rho_{2N} \ll \cdots \ll \rho_{NN} = 1$. The order of magnitudes of the ratios of layer densities allow us to conduct a parametric analysis. The smallness of the nondimensional quantities ρ_{iN} permit certain terms to be eliminated in the exact formulation of Green's function to improve the speed of calculations within acceptable accuracy. To identify the terms to be omitted, the kernel, i.e., solution to Eq. (8), should be expressed explicitly. To this end, we exploit Cramer's rule which expresses the each coefficient in Eq. (8) in terms of ratio of determinants as given by

$$R_N = \frac{|E_N|}{|\Delta_N|}. \tag{13}$$

The determinants of matrices E_N and Δ_N involve the product of ratios of layer densities with different order of magnitudes. Once the coefficients are expressed explicitly, the parametric analysis leads to the elimination of the asymptotically smaller terms from the determinants in the numerator and denominator using the following formula:

$$g = \begin{cases} \rho_{12} K_{z_2}, & N = 2 \\ \displaystyle\sum_{i_k=k+1}^{k+2} \cdots \sum_{i_1=2}^{3} (-1)^{N-1+i_k} s_{N-1 i_k} (-1)^{N-2+i_{k-1}} s_{N-2 i_{k-1}} \\ \quad \cdots (-1)^{2+i_1} s_{2 i_1} \det\left(\left(\left((B)_{2 i_1} \cdots \right)_{N-1 i_k} \right)_{NN} \right), & N \geq 3, \end{cases} \tag{14}$$

where $k = 1, \ldots, N-2$.

The matrix B within the nested parenthesis denote the minors of the matrix where the rows and the columns corresponding to the subscript are deleted from both E_N and Δ_N defined in Eq. (13). Starting from $2N-2$ by $2N-2$ matrices in Eq. (14), this reduction process is continued recursively until the size of the reduced matrix is $N \times N$. The constants s_{ij} denote the entries of the reduced matrix in each step. The terms to be omitted are obtained as the final expansion of the sum given in Eq. (14). Omitting the terms given in Eq. (14) from the coefficient of Green's function (1), we arrive at the so-called *reduced Green's function*.

The analysis presented above permits an analytical inspection of the (reflection-transmission coefficients) determinant of the Green's functions, which is now in shortened form due to the omission of asymptotically smaller quantities, particularly the ratios of densities. The simplified coefficients so obtained elicit efficient and faster computation times of integrals of Green's functions.

https://doi.org/10.1121/10.0011547

IV. NUMERICAL RESULTS

In this section, we present numerical examples to discuss the efficiency of the proposed Green's function. In all examples, the frequency is considered as 1 MHz and the corresponding wavelength is $\lambda = 16 \times 10^{-4}$ m. The source is located at $(x', z') = (2\lambda, 2\lambda)$ unless otherwise stated. The measurement point is being kept in the first layer at $x = 2\lambda$ and z is varied from 2.001λ to 11λ. In the examples of three and four layered media, the thickness for normalization is taken as $d_1 = |h_2 - h_1|$, whereas for two-layered media, it is taken as the distance between the source and the layer. Wolfram MATHEMATICA 11 is used in the computations.

A. Two-layered media

As a first example, we consider the simplest configuration, that is a two-layered medium. The densities and sound velocities are taken $c_1 = 1600$ m/s, $c_2 = 1645$ m/s, and $\rho_1 = 100$ g/cm^3 and $\rho_2 = 1000$ g/cm^3 for layer 1 and layer 2, respectively. Thus, the ratio of densities becomes small and has the value $\rho_{12} = 0.1 \ll 1$.

Having the source and the measurement points in the first layer, the Green's function G_{11} is calculated with the coefficient R_2 which is given as

$$R_2 = \frac{K_{z_1} - \rho_{12} K_{z_2}}{K_{z_1} + \rho_{12} K_{z_2}}. \tag{15}$$

As it is seen, both the numerator and the denominator consist of the small parameter ρ_{12}. By neglecting it from both numerator and denominator, the coefficient R_2 is reduced to 1. This means that a very small amount of transmission to the second medium occurs, and so it can be ignored, all acoustic waves are reflected back to the first medium. This modification can be interpreted as changing to boundary conditions from natural continuity condition to the "sound hard" boundary condition in the reduced Green's function. The absolute values of the reduced Green's function and the exact one are calculated as a function of the distance $|z - z'|$ and are depicted in Fig. 2 which demonstrates a favourable agreement. In order to make quantitative comparison, we also calculate the relative error defined as

$$\text{Error} = \frac{|G_{\text{exact}} - G_{\text{reduced}}|}{|G_{\text{exact}}|} \tag{16}$$

and present it in Fig. 3. It is seen that the error stays the same in the whole distance range from near field to far field. The average computation time of the reduced Green's function for a single point, $|z - z'| = 0.2\lambda$, is 0.1058 s whereas it increases to 0.1541 s for the exact one. It should be emphasized that the small difference in calculation times for the reduced and exact Green's function will apparently become significant when a recursive calculation will be required to obtain a larger set of data points commonly encountered in tomographic imaging algorithms.

B. Three-layered media

We examine the efficiency of the reduced Green's function in a three-layered medium with $N = 3$, see Fig. 1. The densities and the velocities of the layers are, respectively, $\rho_1 = 100$ g/cm^3, $\rho_2 = 700$ g/cm^3, $\rho_3 = 1000$ g/cm^3, $c_1 = 1600$ m/s, $c_2 = 1645$ m/s, and $c_3 = 1675$ m/s for layer 1, layer 2 and layer 3. The thickness of the second layer is taken as $d_1 = 16 \times 10^{-4}$ m. The Green's function G_{11} is calculated by solving the system (8) for $N = 3$. The coefficient appearing the Green's function is given by

$$R_3 = \frac{E_3}{\Delta_3}, \tag{17}$$

where E_3 and Δ_3 are given, respectively, by

$$E_3 = -\cosh(K_{z_2}) K_{z_2} (\rho_{13} K_{z_3} + K_{z_1}) + \sinh(K_{z_2})(\rho_{23} K_{z_1} K_{z_3} + \rho_{12} K_{z_2}^2), \tag{18}$$

$$\Delta_3 = \cosh(K_{z_2}) K_{z_2} (\rho_{13} K_{z_3} - K_{z_1}) + \sinh(K_{z_2})(\rho_{23} K_{z_1} K_{z_3} - \rho_{12} K_{z_2}^2). \tag{19}$$

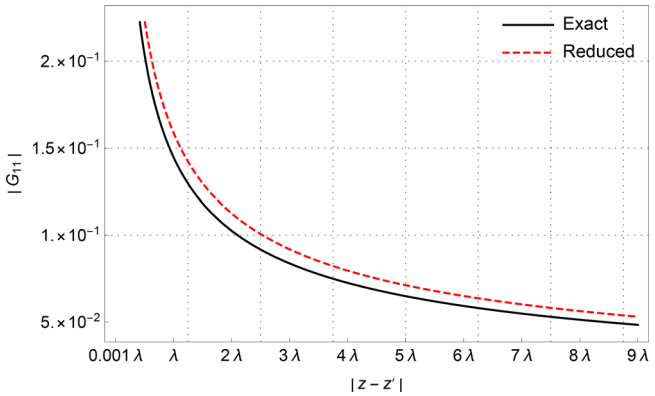

FIG. 2. (Color online) Comparison of exact and reduced Green's functions for a two layered media for $\rho_{12} = 0.1$.

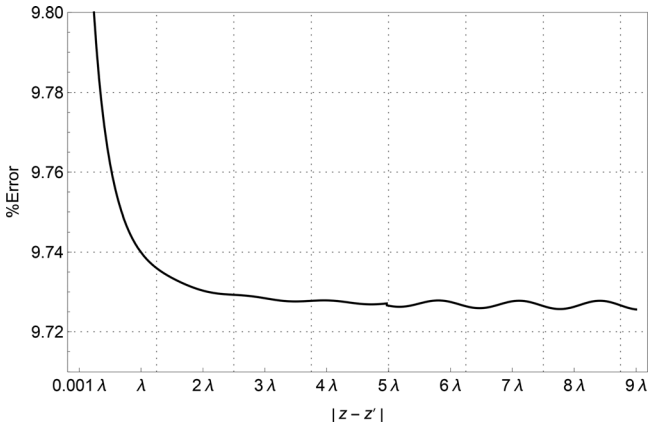

FIG. 3. Relative error of exact and reduced formulations for a two-layered media for $\rho_{12} = 0.1$.

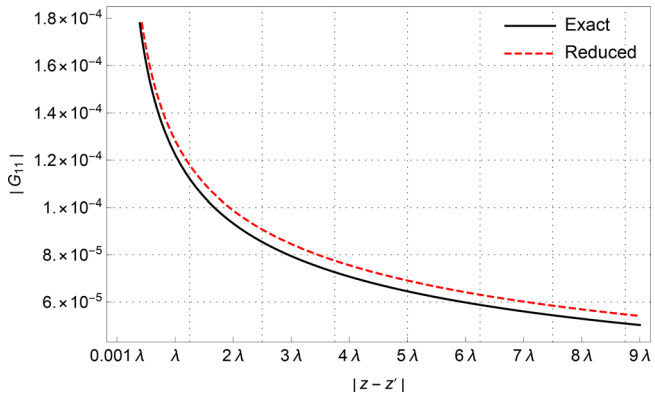

FIG. 4. (Color online) Comparison of exact and reduced Green's functions for a three layered media for $\rho_{13} = 0.1$, for $(x, x') = (2\lambda, 2\lambda)$.

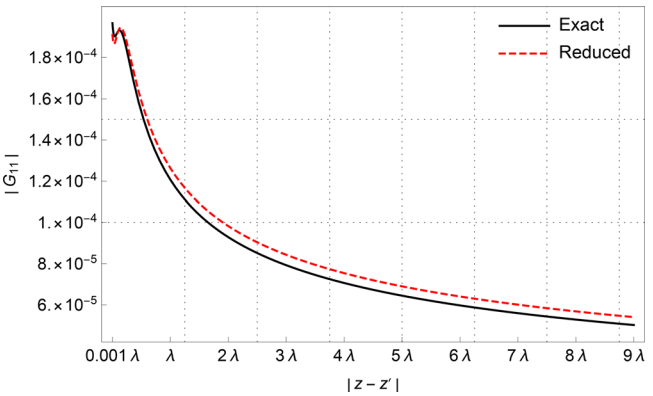

FIG. 6. (Color online) Comparison of exact and reduced Green's functions for a three layered media for $\rho_{13} = 0.1$, for $(x, x') = (2.2\lambda, 2\lambda)$.

Since the densities for the considered case are ordered as $\rho_1 \ll \rho_2 \ll \rho_3$, the smallest parameter becomes $\rho_{13} = \rho_1/\rho_3$ and its value is $\rho_{13} = 0.1$. We may, hence, omit the terms containing ρ_{13}, which can also be determined by Eq. (14), from the expressions (18) and (19) simultaneously thereby obtaining the reduced Green's function. Looking closely to the terms containing ρ_{13}, it can be seen that these terms are responsible from some of multiple reflections in bounded region between the first and the third medium. Due to the high contrast between the two media, this multi reflection effect is small enough to be neglected.

Figure 4 exhibits the numerical comparison of the reduced and exact formulations of Green's functions with respect to the distance $|z - z'|$ for $\rho_{13} = 0.1$, for $(x', z') = (2\lambda, 2\lambda)$. Once again, there is a remarkable coincidence of exact and approximate forms. Near field computation times for a single point $|z - z'| = 0.2\lambda$ of the reduced and exact formulations are 0.2080 and 0.2114 s, respectively. In the far field, $|z - z'| = 3\lambda$, they are calculated, respectively, as 0.2466 and 0.2696 s. A decrease in computation time is clearly observed for the reduced Green's function. The graph of the relative error between exact and reduced Green's functions is displayed in Fig. 5, which is bounded by 8% for all distance ranges. In order to investigate the effect of source and observation point location, oblique observation are considered by taking the source and measurement locations as $(x, x') = (2.2\lambda, 2\lambda)$. The function, G_{11}, for three layered media and error graph are presented in Figs. 6 and 7, respectively. As it is seen, oblique observation results are almost the same as with previous measurement setups where the source and observation are on the same line, perpendicular to the layer, given in Figs. 4 and 5. Hence, the relative positions of the source and observation points has no discernible influence on the accuracy of proposed reduced Green's function.

In Tables I and II, the relative error between exact and reduced formulations are presented for a three-layered media for various ρ_{13} ratios both in near and far fields. Here, the density ρ_1 is fixed at $\rho_1 = 100\,\text{g/cm}^3$ and ρ_3 varies accordingly as determined in the first rows of Tables I and II.

It is demonstrated in Tables I and II that the smaller density ratios result in smaller errors. When density ratios is less than 0.1, the terms may be neglected in the reflection coefficient(s) in both near and far fields which may be taken as a threshold with an error around 1% and 3%, respectively.

C. Four-layered media

In a four-layered media, we examine the efficiency of the reduced Green's function for two different setups: in the

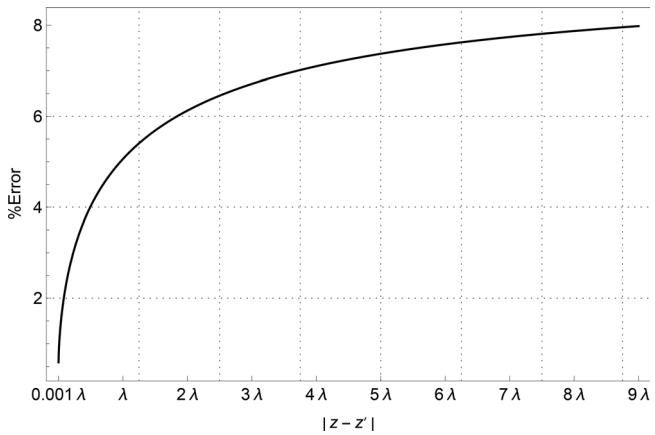

FIG. 5. Relative error of exact and reduced formulations for a three-layered media for $\rho_{13} = 0.1$.

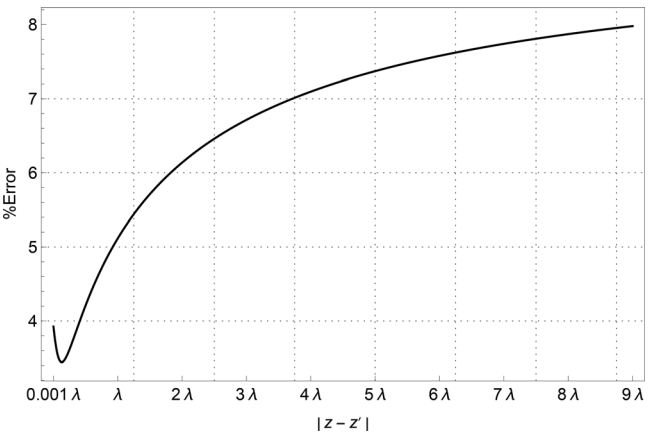

FIG. 7. Relative error of exact and reduced formulations for a three-layered media for $\rho_{13} = 0.1$, for $(x, x') = (2.2\lambda, 2\lambda)$.

https://doi.org/10.1121/10.0011547

TABLE I. Exact and reduced Green's function values and relative error against varied ratio of densities ρ_{13} in three layered medium for $|z-z'|=0.001\lambda$.

ρ_{13}	0.5	0.4	0.3	0.2	0.1	0.05	0.025	0.01
Exact ($\times 10^{-4}$)	4.83	4.87	4.91	4.91	5.01	5.04	5.05	5.06
Reduced ($\times 10^{-4}$)	5.07	5.07	5.07	5.07	5.07	5.07	5.07	5.07
Error (%)	4.82	4.04	3.19	2.24	1.16	0.60	0.30	0.12

first one, both the source and measurement point are located in the first layer, requiring the computation of G_{11}. In the second setup, the source and measurement point are located different layers where source in the first layer and measurement is in the third layer requiring the computation of G_{13}. We also investigate the effect on the order of density magnitudes in both setups by sorting them differently in two subcases.

In all cases, the sound velocities are taken as $c_1 = 1600$, $c_2 = 1645$, $c_3 = 1675$, $c_4 = 1650$ m/s.

Setup 1: In this first setup, both source and measurement points are located in the first layer. The thicknesses of the second and third layers are taken as 16×10^{-4} m. The reflection coefficient in the Green's function G_{11}, therefore, takes the following form:

$$R_4 = \frac{E_4^{(1)}}{\Delta_4}, \tag{20}$$

where $E_4^{(1)}$ and Δ_4 are given as

$$\begin{aligned} E_4^{(1)} = {} & K_{z_2}\cosh(K_{z_2})\Big(K_{z_3}^2\cosh((1-\mathcal{H}_3)K_{z_3}) \\ & \times (K_{z_1} - \rho_{14}K_{z_4}) + \sinh((1-\mathcal{H}_3)K_{z_3}) \\ & \times \left(\rho_{34}K_{z_1}K_{z_4} - \rho_{13}K_{z_3}^2\right)\Big) + \sinh(K_{z_2}) \\ & \times \Big(K_{z_3}\cosh((1-\mathcal{H}_3)K_{z_3})(\rho_{12}K_{z_2}^2 - \rho_{24}K_{z_1}K_{z_4}) \\ & + \sinh((1-\mathcal{H}_3)K_{z_3})(K_{z_2}^2 - \rho_{23}K_{z_1}K_{z_3}^2)\Big), \end{aligned} \tag{21}$$

$$\begin{aligned} \Delta_4 = {} & K_{z_2}\cosh(K_{z_2})\Big(K_{z_3}^2\cosh((1-\mathcal{H}_3)K_{z_3}) \\ & \times (K_{z_1} + \rho_{14}K_{z_4}) + \sinh((1-\mathcal{H}_3)K_{z_3}) \\ & \times \left(\rho_{13}K_{z_3}^2 + \rho_{34}K_{z_1}K_{z_4}\right)\Big) + \sinh(K_{z_2}) \\ & \times \Big(K_{z_3}\cosh((1-\mathcal{H}_3)K_{z_3})(\rho_{12}K_{z_2}^2 + \rho_{24}K_{z_1}K_{z_4}) \\ & + \sinh((1-\mathcal{H}_3)K_{z_3})(\rho_{23}K_{z_1}K_{z_3}^2 + \rho_{12}\rho_{34}K_{z_2}^2K_{z_4})\Big). \end{aligned} \tag{22}$$

TABLE II. Exact and reduced Green's function values and relative error against varied ratio of densities ρ_{13} in three layered medium $|z-z'|=7\lambda$.

ρ_{13}	0.5	0.4	0.3	0.2	0.1	0.05	0.025	0.01
Exact ($\times 10^{-5}$)	4.42	4.66	4.93	5.24	5.60	5.80	5.90	5.97
Reduced ($\times 10^{-5}$)	6.01	6.01	6.01	6.01	6.01	6.01	6.01	6.01
Error (%)	36	29	21	14	7	3.72	1.86	0.74

For the Green's function G_{11}, let us consider two cases.

In the first case, the densities are given as $\rho_1 = 100\,\text{g/cm}^3$, $\rho_2 = 500\,\text{g/cm}^3$, $\rho_3 = 700\,\text{g/cm}^3$, $\rho_4 = 1000\,\text{g/cm}^3$ which corresponds to $\rho_1 \ll \rho_2 \ll \rho_3 \ll \rho_4$, giving the smallest parameter as ρ_{14}. The reduced Green's function is obtained by neglecting the containing the smallest term ρ_{14} using the formula (14).

The results of the numerical comparisons are presented in Fig. 8 and a remarkable agreement is observed for all points both in the near and far fields.

The computation time of the reduced Green's function for a single point in the near field, $|z-z'|=0.2\lambda$, is 0.3613 s, whereas it increases to 0.4203 s for the exact one. In the case of far field for $|z-z'|=3\lambda$, they are given as 0.3662 and 0.4062 s. A notable decrease is evident in the computation times even for a single point.

Now for the second case, we consider different densities where $\rho_1 = 500\,\text{g/cm}^3$, $\rho_2 = 100\,\text{g/cm}^3$, $\rho_3 = 1000\,\text{g/cm}^3$, $\rho_4 = 700\,\text{g/cm}^3$ corresponding to $\rho_2 \ll \rho_1 \ll \rho_4 \ll \rho_3$ which has different descending order from what has been considered so far. The smallest term, in this case, becomes ρ_{23} and neglecting, once again, the terms containing ρ_{23} from Eqs. (21) and (22), the reduced Green's function is straightforwardly obtained. The exact and reduced Green's functions are compared in Fig. 9. Although an identical plot is displayed to the previous case, there appears a slight shift of the reduced Green's function due to the different ordering of the layer densities. The CPU times are calculated as 0.3355 and 0.3358 s in the near field at $|z-z'|=0.2\lambda$ corresponding to reduced and exact formulations, whereas they are given as 0.3776 and 0.3911 s, respectively, in the far field at $|z-z'|=3\lambda$. The relative errors, displayed in Fig. 10, in each case, diminish in the far field and become bounded by 8%.

***Setup 2*:** In this setup, the source and measurement points are taken in different layers, the source being in the first layer at $z' = 2\lambda$ m and the measurement point being in the third layer. The thicknesses of the second and third layers are taken as 16×10^{-4} and 48×10^{-4} m, respectively. The structure of the exact Green's function, now, takes the form

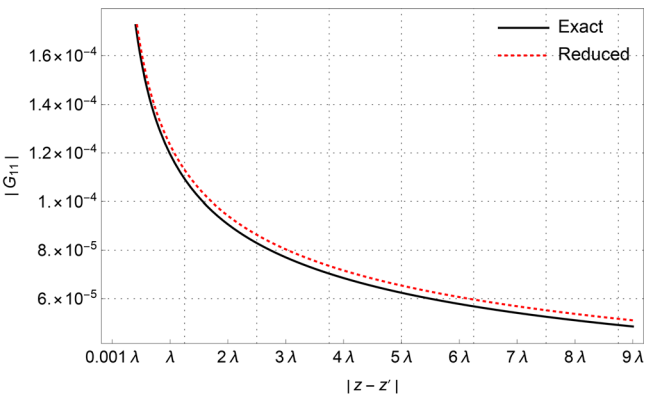

FIG. 8. (Color online) Setup 1: Comparison of exact and reduced Green's functions for a four-layered media for $\rho_{14} = 0.1$.

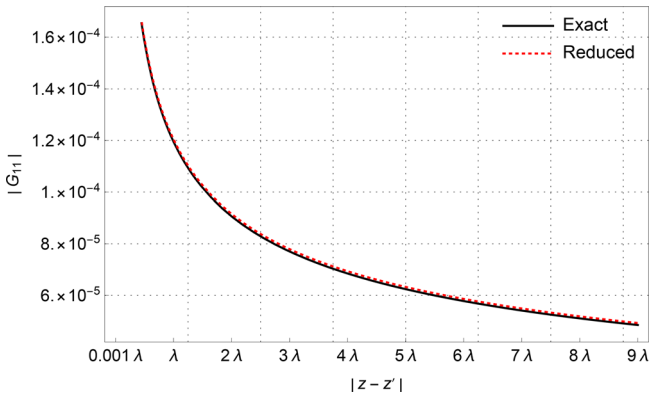

FIG. 9. (Color online) Setup 1: Comparison of exact and reduced Green's functions for a four-layered media for $\rho_{23} = 0.1$.

$$G_{13} = \frac{1}{2\pi}\int_0^{\infty} (C_1^{(3)}\sinh(k_{z_3}z) + C_2^{(3)}\cosh(k_{z_3}z))\frac{\cos(k_x|x-x'|)}{k_{z_1}}dk_x, \tag{23}$$

where

$$C_1^{(3)} = \frac{E_4^{(3)}}{\Delta_4}, \quad C_2^{(3)} = \frac{F_4^{(3)}}{\Delta_4}, \tag{24}$$

$$E_4^{(3)} = 2e^{-z'K_{z_1}}K_{z_1}K_{z_2}(-K_{z_4}\rho_{34}\cosh(\mathcal{H}_3K_{z_3}) + K_{z_3}\sinh(K_{z_3}\mathcal{H}_3)), \tag{25}$$

$$F_4^{(3)} = 2e^{-z'K_{z_1}}K_{z_1}K_{z_2}(-K_{z_3}\cosh(\mathcal{H}_3K_{z_3}) + \rho_{34}K_{z_4}\sinh(K_{z_3}H_3)). \tag{26}$$

We, again, consider two sub cases. In the first sub case, we take the densities in order of increasing magnitudes, i.e., $\rho_1 = 100$ g/cm^3, $\rho_2 = 500$ g/cm^3, $\rho_3 = 700$ g/cm^3, $\rho_4 = 1000$ g/cm^3, which corresponds to $\rho_1 \ll \rho_2 \ll \rho_3 \ll \rho_4$, giving the smallest parameter as ρ_{14}. This gives the reduced form of G_{13} omitting the smallest terms containing ρ_{14} in the expressions (22), (25), and (26) on using Eq. (14).

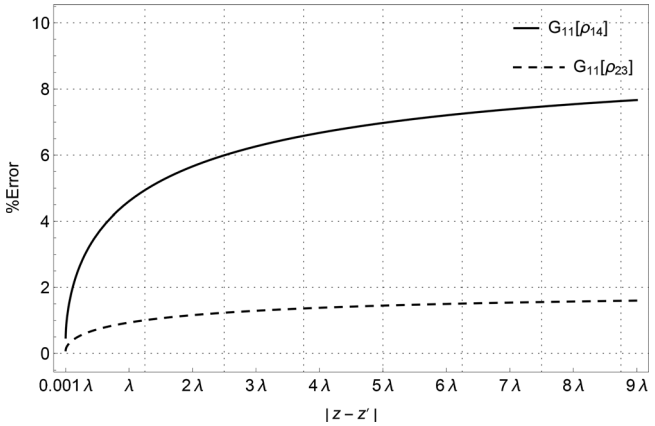

FIG. 10. Setup 1: Relative errors of exact and reduced formulations for a four-layered media for $\rho_{14} = 0.1$ (solid line) and $\rho_{23} = 0.1$ (dashed line).

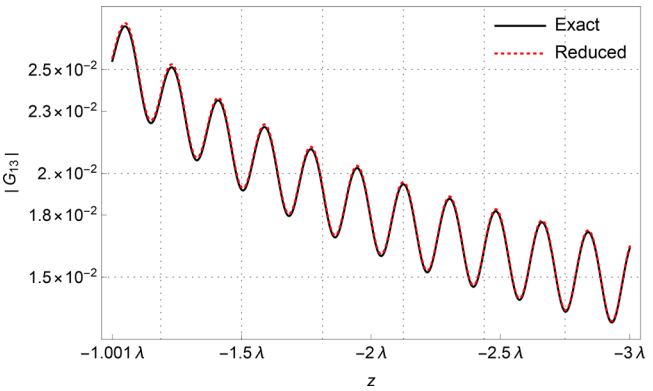

FIG. 11. (Color online) Setup 2: Comparison of exact and reduced Green's functions for a four-layered media for $\rho_{14} = 0.1$.

In the second sub case, we take $\rho_2 \ll \rho_1 \ll \rho_4 \ll \rho_3$, by assigning $\rho_1 = 500$ g/cm^3, $\rho_2 = 100$ g/cm^3, $\rho_3 = 1000$ g/cm^3, $\rho_4 = 700$ g/cm^3. As before, the reduced Green's function is obtained by neglecting the asymptotically smallest term ρ_{23} appearing in the coefficients (22), (25), and (26).

Both Figs. 11 and 12 illustrate the numerical comparisons from the measurement point located in the third layer coordinate at $z = -1.001\lambda$ to $z = -3\lambda$. The horizontal axis is labeled in terms of the increasing distance between source and measurement location. It is clear from both figures that as the distance to source increases, the magnitude of Green's function decays. It should be noted that the oscillatory behavior is a result of the existence of downward and upward waves in layered media and the width of oscillation mainly depends on the thicknesses of layers. The exact and reduced forms of Green's functions overlap remarkably well in both sub cases. As a consequence of the parametric analysis employed in deriving the reduced Green's functions, there is also a gain in the CPU times in both sub cases; the reduced ones given by 0.244556, 0.235901 s at $z = -32 \times 10^{-4}$ and the exact ones given by 0.248239, 0.237248 s at $z = -32 \times 10^{-4}$, for first and second sub cases, respectively. The relative errors displayed in Fig. 13 for each sub case are well below 1% and confirm the remarkable agreement between the exact and reduced formulations. The comparison of calculation times of exact and reduced Green's functions in all cases

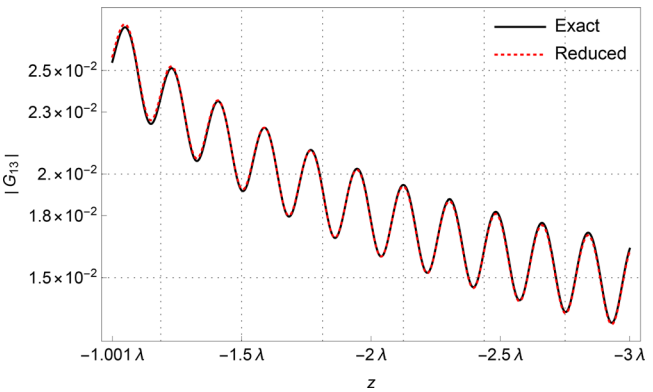

FIG. 12. (Color online) Setup 2: Comparison of exact and reduced Green's functions for a four-layered medium for $\rho_{23} = 0.1$.

https://doi.org/10.1121/10.0011547

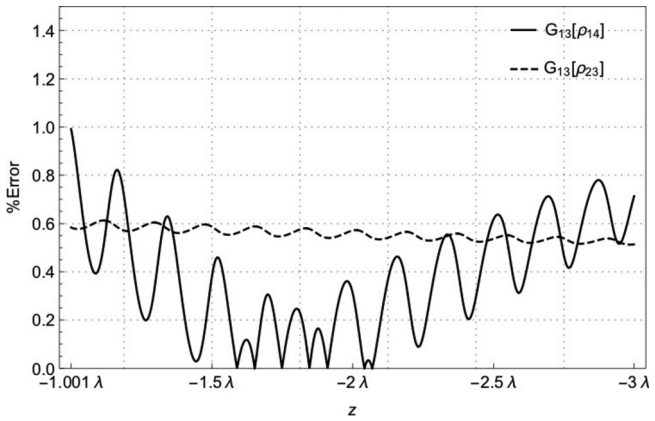

FIG. 13. Setup 2: Relative errors of exact and reduced formulations for a four-layered media for $\rho_{14} = 0.1$ (solid line) and $\rho_{23} = 0.1$ (dashed line).

considered above in both near and far field regions are presented in Tables III and IV. It is clearly observed that, even for a single point, the CPU times decrease in case of reduced Green's functions which proves to be an important advantage in imaging algorithms where the Green's function is required to be computed recursively. However, we should note that as the number of layer increases, the improvement in computational times decreases. The reason for this can be explained as that as the number of layer increases, the number of terms in Green's function increases and thus, the effect of ignorance of leading order term diminishes.

V. CONCLUSION

In this paper, a parametric analysis is applied to derive reduced forms of acoustic Green's functions for a layered media. Taking advantage of the different order of magnitudes of the layer densities, a small parameter is introduced in the formulation of Green's functions which, then, enable the reduction of the kernels resulting in *reduced* Green's functions. Comprehensive numerical investigations are conducted in layered medium by varying the number of layers and sorting the orders of densities. The accuracy of the reduced Green's functions are tested against the exact ones taking into account the distance between the source and measurement location. The results affirm that the method employed facilitates faster and efficient calculation times and, thus, proves to be an effective approach in the simplification of Green's functions.

TABLE III. CPU time in seconds per point for near and far field ranges for G_{11}.

	Exact Green's	Reduced Green's	ρ_{nm}	Number of layers
	0.1541	0.1058	$\rho_{12} \ll 1$	2-Layered
	0.2114	0.2080	$\rho_{13} \ll 1$	3-Layered
$\lvert z - z' \rvert = 0.2\lambda$	0.4203	0.3613	$\rho_{14} \ll 1$	4-Layered
	0.3358	0.3355	$\rho_{23} \ll 1$	4-Layered
	0.2596	0.1067	$\rho_{12} \ll 1$	2-Layered
	0.2696	0.2466	$\rho_{13} \ll 1$	3-Layered
$\lvert z - z' \rvert = 3\lambda$	0.4062	0.3662	$\rho_{14} \ll 1$	4-Layered
	0.3911	0.3776	$\rho_{23} \ll 1$	4-Layered

TABLE IV. CPU time in seconds per point for far field range for G_{13}.

	Exact Green's	Reduced Green's	ρ_{nm}	Number of layers
$\lvert z - z' \rvert = 4\lambda$	0.248239	0.244556	$\rho_{14} \ll 1$	4-Layered
	0.237248	0.235901	$\rho_{23} \ll 1$	4-Layered

ACKNOWLEDGMENTS

This work was supported by TUBITAK of Turkey through the ARDEB-1001 Program under Grant No. 119E624.

[1]F. R. DiNapoli and R. L. Deavenport, "Theoretical and numerical Green's function field solution in a plane multilayered medium," J. Acoust. Soc. Am. **67**(1), 92–105 (1980).
[2]W. C. Chew, *Waves and Fields in Inhomogeneous Media (Electromagnetic Waves)* (IEEE Computer Society Press, Piscataway, NJ, 1995).
[3]B. Uzun and H. Yücel, "An inverse source problem connected with thermoacoustic imaging in multi-layer planar medium," J. Math. Imag. Vision **61**(6), 874–884 (2019).
[4]R. R. Boix, A. L. Fructos, and F. Mesa, "Closed-form uniform asymptotic expansions of Green's functions in layered media," IEEE Trans. Ant. Propag. **58**(9), 2934–2945 (2010).
[5]K. A. Michalski, "Extrapolation methods for Sommerfeld integral tails," IEEE Trans. Ant. Propag. **46**(10), 1405–1418 (1998).
[6]D. Fang, J. Yang, and G. Delisle, "Discrete image theory for horizontal electric dipoles in a multilayered medium," in *IEEE Proceedings H-Microwaves, Antennas and Propagation*, IET (1988), Vol 135, pp. 297–303.
[7]G. Dural and M. I. Aksun, "Closed-form Green's functions for general sources and stratified media," IEEE Trans. Microw. Theory Tech. **43**(7), 1545–1552 (1995).
[8]M. Aksun, "A robust approach for the derivation of closed-form Green's functions," IEEE Trans. Microw. Theory Tech. **44**(5), 651–658 (1996).
[9]E. Simsek, Q. H. Liu, and B. Wei, "Singularity subtraction for evaluation of Green's functions for multilayer media," IEEE Trans. Microw. Theory Tech. **54**(1), 216–225 (2006).
[10]R. R. Boix, F. Mesa, and F. Medina, "Application of total least squares to the derivation of closed-form Green's functions for planar layered media," IEEE Trans. Microw. Theory Tech. **55**(2), 268–280 (2007).
[11]A. Alparslan, M. I. Aksun, and K. A. Michalski, "Closed-form Green's functions in planar layered media for all ranges and materials," IEEE Trans. Microw. Theory Tech. **58**(3), 602–613 (2010).
[12]Y. Liu, L.-W. Li, T.-S. Yeo, and M.-S. Leong, "Application of DCIM to MPIE-MOM analysis of 3D PEC objects in multilayered media," IEEE Trans. Antennas Propag. **50**(2), 157–162 (2002).
[13]M. Van Blaricum and R. Mittra, "A technique for extracting the poles and residues of a system directly from its transient response," IEEE Trans. Antennas Propag. **23**(6), 777–781 (1975).
[14]Y. Hua and T. K. Sarkar, "Generalized pencil-of-function method for extracting poles of an EM system from its transient response," IEEE Trans. Antennas Propag. **37**(2), 229–234 (1989).
[15]V. I. Okhmatovski and A. C. Cangellaris, "A new technique for the derivation of closed-form electromagnetic Green's functions for unbounded planar layered media," IEEE Trans. Antennas Propag. **50**(7), 1005–1016 (2002).
[16]V. I. Okhmatovski and A. C. Cangellaris, "Evaluation of layered media green's functions via rational function fitting," IEEE Microw. Wireless Compon. Lett. **14**(1), 22–24 (2004).

[17]B. T. Cox, S. Kara, S. R. Arridge, and P. C. Beard, "k-space propagation models for acoustically heterogeneous media: Application to biomedical photoacoustics," J. Acoust. Soc. Am. **121**(6), 3453–3464 (2007).
[18]J. Kaplunov, D. Prikazchikov, and O. Sergushova, "Multi-parametric analysis of the lowest natural frequencies of strongly inhomogeneous elastic rods," J. Sound Vib. **366**, 264–276 (2016).
[19]L. Prikazchikova, Y. E. Aydin, B. Erbaş, and J. Kaplunov, "Asymptotic analysis of an anti-plane dynamic problem for a three-layered strongly inhomogeneous laminate," Math. Mech. Solids **25**(1), 3–16 (2020).
[20]J. Kaplunov, L. Khajiyeva, M. Martyniuk, and A. Sergaliyev, "On the dynamics of drilling," Int. J. Eng. Sci. **146**, 103184 (2020).